

## Coexistence of dimerization and long-range magnetic order in the frustrated spin-chain system $\text{LiCu}_2\text{O}_2$ : Inelastic light scattering study

K.-Y. Choi,<sup>1</sup> S. A. Zvyagin,<sup>2</sup> G. Cao,<sup>3</sup> and P. Lemmens<sup>1,4</sup><sup>1</sup>*Physikalisches Institut, RWTH Aachen, 52056 Aachen, Germany*<sup>2</sup>*National High Magnetic Field Laboratory, 1800 East Paul Dirac Drive, Tallahassee, Florida 32310, USA*<sup>3</sup>*Department of Physics and Astronomy, University of Kentucky, Lexington, Kentucky 40506, USA*<sup>4</sup>*MPI for Solid State Research, 70569 Stuttgart, Germany*

(Received 6 May 2003; revised manuscript received 29 October 2003; published 22 March 2004)

Raman scattering studies of the frustrated spin chain system  $\text{LiCu}_2\text{O}_2$  are reported. Two transitions into a magnetically ordered phase (taken place at temperatures  $\sim 9$  and  $\sim 24$  K) have been confirmed from the analysis of optical properties of the samples. Interestingly, two different magnetic excitations, seen at 100 and  $110\text{ cm}^{-1}$  in the magnetically ordered phase superimpose each other independently, indicating a coherent coexistence of long-range magnetic order and dimerization. The observed phenomenon is attributed to magnetostructural peculiarities of  $\text{LiCu}_2\text{O}_2$  leading to the intrinsic presence of magnetic/nonmagnetic impurities on a nanometer scale. In particular, magnetic impurities play a significant role in driving the transition from an incommensurate state to a Néel ordered one at 9 K.

DOI: 10.1103/PhysRevB.69.1044XX

PACS number(s): 75.40.-s, 78.30.-j, 75.10.Pq, 75.80.+q

Theoretical and experimental investigations of low-dimensional spin systems with frustration and dimerization have been boosted by the discovery of the inorganic spin-Peierls system  $\text{CuGeO}_3$ .<sup>1</sup> Such a frustrated spin-chain system shows a rich phase diagram, including both gapped and gapless phases,<sup>2</sup> as well as disorder-induced long-range ordering, coexisting with a dimerized state.<sup>3</sup> Variational calculations suggest that the resonating-valence-bond character of spin correlations at short distances can be responsible for the enhancement of antiferromagnetic (AFM) correlations near vacancies,<sup>4,5</sup> that eventually results in long-range AFM order, locally coexisting with the disordered dimerized phase. Such a coexistence was observed in some other doped systems with reduced dimensionality [for instance, in highly hole-doped chain material  $\text{Sr}_{0.73}\text{CuO}_2$  (Ref. 6)] and appears to be a fundamental property of low-dimensional quantum spin systems.

$\text{LiCu}_2\text{O}_2$  can be regarded as a realization of a  $S = 1/2$  spin chain with competing nearest- and next-nearest-neighbor interactions.<sup>7-11</sup> This compound has an orthorhombic crystal structure of a space group  $Pnma$  with the lattice parameters  $a = 5.72$ ,  $b = 2.86$ , and  $c = 12.4$  Å.<sup>7</sup> There are monovalent and bivalent copper ions in the unit cell. Magnetic  $\text{Cu}^{2+}$  ions form a double chain along the  $b$  axis, which is separated from each other by both Li ions and planes with nonmagnetic  $\text{Cu}^+$  ions. The two separate Cu chains within the double-chain structure are coupled via a nearly  $90^\circ$  oxygen bond along the  $c$  axis. At elevated temperatures high-field electron spin resonance (ESR) gives evidence for a spin singlet state with spin gap of  $\Delta \sim 72$  K.<sup>10</sup> Interestingly, upon cooling a spin singlet state transits into a long-range ordered state with helimagnetic structure at  $T_{c_1} \sim 24$  K.<sup>11</sup> Some bulk measurements point to the presence of a second low-temperature transition with a collinear AFM structure at  $T_{c_2} \sim 9$  K.<sup>10</sup> Both transitions are attributed to an intrinsic nonstoichiometry and the effect of nonmagnetic and/or magnetic impurities.<sup>10,11</sup> However, the exact origin is not yet

clear. In addition, with decreasing temperature a reduction of orthorhombic strain has been observed.<sup>8</sup> These magnetostructural peculiarities of  $\text{LiCu}_2\text{O}_2$  provide a good opportunity to investigate the influence of a variety of magnetic and nonmagnetic impurities on magnetic property of a frustrated spin chain system.

Raman spectroscopy has proven to be an extremely powerful technique to probe magnetic excitations and spin-lattice interactions in a low-dimensional spin system with unprecedented precision.<sup>2</sup> The main motivation of this work is using Raman spectroscopy technique to study the nature of ground state and the magnetostructural peculiarities in quantum AFM  $\text{LiCu}_2\text{O}_2$ . In the following we will show the coherent coexistence of long-range ordered states with dimerized state induced by nanoscale defects. Further, we propose a possible mechanism for a disorder-induced long-range ordering in the studied system.

The single crystals were grown using a self-flux method and characterized by a microstructural analysis and thermodynamic measurements as described in Ref. 10. The single crystals are microscopically twinned and contain  $\text{LiCuO}$ -impurity phase. Raman spectra were measured in a quasi-backscattering geometry with the excitation line  $\lambda = 514.5$  of a  $\text{Ar}^+$  laser with the power of 10 mW and were analyzed by a DILOR-XY spectrometer and a nitrogen cooled charge-coupled device detector.

Figure 1 displays Raman spectra in parallel ( $xx$ ) and crossed ( $xy$ ) polarizations at 3 K as well as at 5 K and room temperature in  $xx$  polarization. Here the  $x$  axis is an arbitrary direction in the  $ab$  plane. Raman spectra in  $xy$  polarization exhibit the same behavior as those in  $xx$  polarization with weaker intensity due to a twinning of the single crystal.<sup>10</sup> Thus, the observed spectra can be regarded as an average of all  $ab$  plane polarizations. Subtracting the acoustic ( $B_{1u} + B_{2u} + B_{3u}$ ) modes the factor group analysis of the space group  $Pnma$  yields the following Raman- and infrared-active modes;  $10A_g(aa,bb,cc) + 5B_{1g}(ab) + 10B_{2g}(ac)$

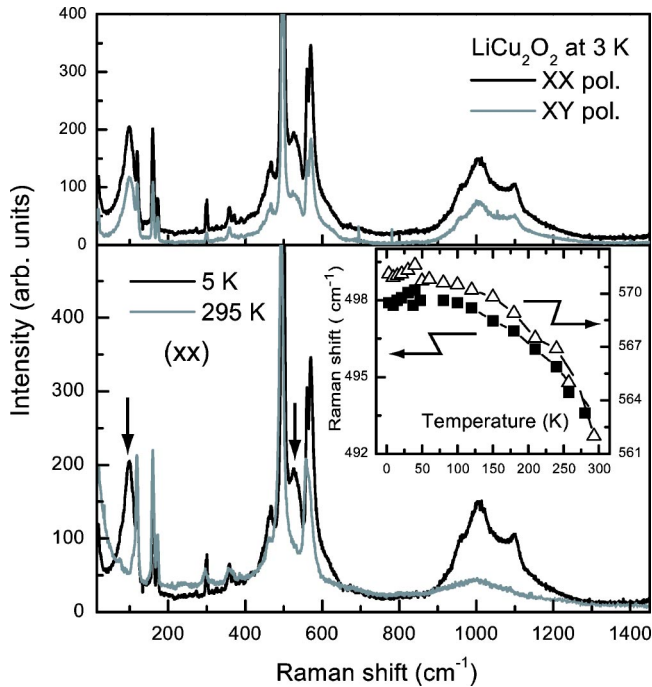


FIG. 1. Raman spectra of  $\text{LiCu}_2\text{O}_2$  in parallel ( $xx$ ) and crossed ( $xy$ ) polarizations at 3 K (upper panel) as well as at low and room temperature in parallel polarization (lower panel). The arrows indicate additional phonon and magnetic signals which appear at low temperature. Inset: Temperature dependence of the 494 and 562  $\text{cm}^{-1}$  phonon modes.

+  $5B_{3g}(bc) + 5A_u + 9B_{1u} + 4B_{2u} + 9B_{3u}$ . At room temperature we observe 12 Raman-active modes out of the maximally expected 15 modes in  $ab$  plane polarizations. A broad band extending from 850 to 1300  $\text{cm}^{-1}$  is an overtone feature of the first-order signals between 400 and 650  $\text{cm}^{-1}$ . This might be due to strong anharmonic lattice interactions and/or resonant scattering.

With decreasing temperature both new phonon modes and magnetic continua show up in an intriguing manner. First, we focus on phonon anomalies which reflect changes of the local symmetry and bond strengths. Upon cooling new phonon modes at 475  $\text{cm}^{-1}$  and 518  $\text{cm}^{-1}$  appear below 55 K and 200 K, respectively. The former temperature corresponds to roughly the exchange constant of  $J \sim 66$  K (Ref. 11) while the latter one is related to the appearance of the spin gap.<sup>10</sup> Note here that the number of the observed 14 modes in the low-temperature region is still smaller than the predicted one (15 modes), suggestive of no reduction of crystal symmetry at low temperatures. In addition, almost all phonon modes become sharp and intense while the Cu-O bending and stretching modes show significant changes as the inset of Fig. 1 displays. Upon cooling the 494  $\text{cm}^{-1}$  and the 562  $\text{cm}^{-1}$  modes undergo an appreciable hardening of 5–8  $\text{cm}^{-1}$  and then saturate around  $T = 55$  K. Upon further cooling they soften slightly while showing a tiny jump at 50 K. Noticeably, a softening takes place around temperature of the exchange constant  $J \sim 66$  K.<sup>11</sup> Thus, a softening below 50 K can be attributed to a renormalization of phonon energy via spin-phonon coupling, similar to the alternating spin-

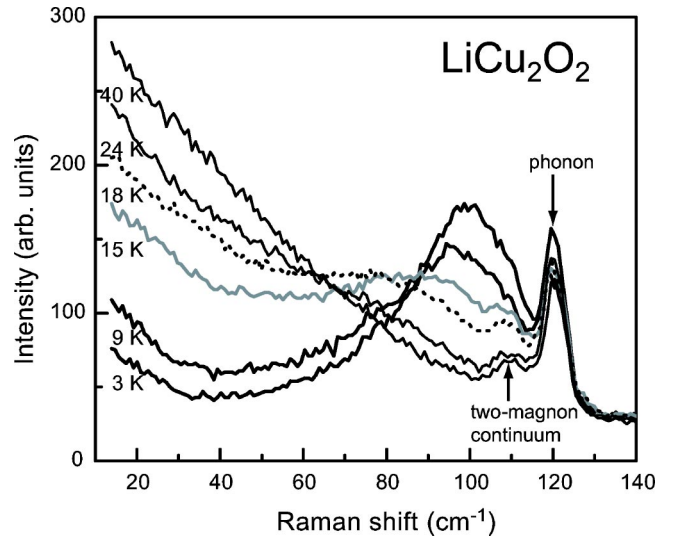


FIG. 2. Low-frequency Raman scattering of  $\text{LiCu}_2\text{O}_2$ . Quasi-elastic scattering and two different kinds of two-magnon continua have been observed.

chain system  $(\text{VO})_2\text{P}_2\text{O}_7$ .<sup>12,13</sup> The smallness of the observed softening is related to the big difference in energy scale between  $J \sim 66$  K and the optical phonon energy of  $\sim 700$  K which mediates the exchange paths along the double chain. High-resolution x-ray diffraction measurements<sup>8</sup> show a substantial increase of orthorhombic strain  $(a-b)/(a+b)$  upon heating. Transition metal oxides may show a decrease of the orthorhombicity with increasing temperature, since thermally activated lattice vibrations reduce the strain. Normally, phonon frequencies shift to higher energy, linewidths broaden, and integrated intensity of some phonon modes decreases. The studied system follows the behavior expected for usual systems despite the opposite behavior of the orthorhombicity as a function of temperature. To clarify the seemingly inconsistency between local and bulk properties detailed studies of structure as a function of temperature are needed.

We will turn now to distinctive features of magnetic excitations observed at low temperatures and low frequencies. As Fig. 2 displays, at 3 K a broad asymmetric continuum around 100  $\text{cm}^{-1}$  is seen. With increasing temperature the continuum shifts to lower energy while damping increases. At the same time, a quasielastic scattering response and a weak continuum around 110  $\text{cm}^{-1}$  develop. Although the crystals are twinned, the dynamics of low-dimensional spin system can be well resolved by Raman spectroscopy. This is because magnetic Raman scattering of low-dimensional systems contributes selectively to the polarization direction in which the incident and scattered light is parallel to the dominant exchange paths. Thus, twinning does not add an essential difficulty to interpreting magnetic signals. To clarify the relation between the magnetic excitations and the structure of magnetic ordering observed in the bulk material we will distinguish three phases following Ref. 10; (I) magnetic ordered phase ( $T < 9$  K, presumably with collinear AFM structure), (II) helimagnetic ordered phase<sup>14</sup> ( $9 \text{ K} < T < 23 \text{ K}$ ), and (III) dimerized phase ( $T > 23 \text{ K}$ ).

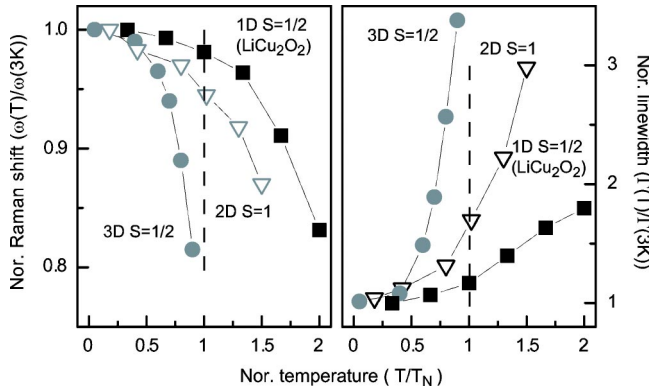


FIG. 3. Comparison of renormalized frequency (left panel) and damping (right panel) of two-magnon continuum as a function of spin number and dimensionality. The higher-dimensional data are taken from Refs. 16 and 17. The dashed vertical line marks a Néel temperature.

In phase I the broad continuum extending from 40 to  $130 \text{ cm}^{-1}$  is observed. This continuum persists as a wing feature of quasielastic scattering up to  $T = 21 \text{ K}$  ( $2.3T_{c_2}$ ). This feature is typical for two-magnon (2M) scattering originating from double spin-flip processes via the exchange mechanism in antiferromagnets with collinear structure.<sup>15</sup> Therefore, we identify phase I to be Néel ordered with  $T_N = T_{c_2} = 9 \text{ K}$ .

The evolution of the 2M spectrum reflects mainly the temperature dependence of short-wavelength magnon energies and lifetimes.<sup>16</sup> Thus, the persistence of 2M scattering to several  $T_N$  can be interpreted in terms of the presence of short-range magnetic fluctuations damped by thermal fluctuations. In Fig. 3 its temperature dependence of the normalized 2M frequency and the full width at half-maximum is presented together with higher dimensional results.<sup>16,17</sup> Magnon-pair energies of  $\text{LiCu}_2\text{O}_2$  [one-dimensional (1D)  $S = 1/2$ ] are renormalized only by 3% at  $T_N$ . In contrast, the magnon-pair spectral weight is renormalized by 25% at  $T_N$  for 3D  $S = 1/2$  systems and by less than 5% for 2D  $S = 1$  systems.<sup>16,17</sup> The damping does scarcely take place at  $T_N$  for  $\text{LiCu}_2\text{O}_2$ . However, it strongly increases as the dimension and spin number increase as the right panel of Fig. 3 displays. The higher dimensionality and spin number are, the larger are changes of spectral weights at an energy scale comparable to the Néel temperature. This is related to the fact that the Néel temperature is not an appropriate energy scale for magnetic excitations in low-dimensional systems. Compared to higher dimensional systems, the robustness of spin-fluctuation dynamics at the energy scale of  $T_N$  confirms the low-dimensional character of the studied system.

The frequency of the 2M peak allows an estimate of the unrenormalized AFM exchange constant between copper spins. The exact determination of the exchange constant in the studied system is impossible because no theoretical calculation for a double-chain system is known. However, one can make a reasonable estimation using not too stringent assumptions. Because of frustrations, the magnetic behavior of  $\text{LiCu}_2\text{O}_2$  lies between 1D and 2D antiferromagnet. In the

2D case, the peak energy of  $2.7 \text{ J}$  imposes a lower boundary of the exchange constant.<sup>18</sup> In frustrated chain systems the one-magnon dispersion is given by  $\omega(k) = J[1 - \alpha \cos(kd)/2]$  with the frustration parameter  $\alpha$  and the chain repeat vector  $d$ .<sup>19</sup> In the noninteracting case 2M scattering is given by twice the magnon density of states. Thus, the peak energy corresponds to  $J(2 + \alpha)$ . If we assume a renormalization of the peak energy due to magnon-magnon interactions by the order of  $J\alpha$ , then an upper boundary of the exchange constant is roughly given by  $2J$ . To conclude, one obtains  $52 \text{ K} < J < 70 \text{ K}$  from the peak energy of  $140 \text{ K}$  ( $= 100 \text{ cm}^{-1}$ ). This value encompasses  $J = 66 \text{ K}$  obtained by a fit of a frustrated chain model to the static susceptibility.<sup>11</sup>

In the following we will discuss the phases II and III. Quasielastic scattering develops in the respective temperature interval. In addition, a weak continuum extending from  $102$  to  $120 \text{ cm}^{-1}$  becomes clearly distinguishable from the broad 2M continuum. This continuum persists up to  $200 \text{ K}$ , that is, into the dimerized phase III. We thus assign the observed signal to a 2M continuum which corresponds to a double spin-flip process of two singlets into a higher singlet state.<sup>2</sup> Since the onset of the continuum corresponds to twice the spin gap, one obtains a spin gap of  $\Delta \approx 73 \text{ K}$ . This value is in excellent agreement with  $\Delta \approx 72 \text{ K}$  from high-field ESR measurements.<sup>10</sup>

However, we find no evidence for the presence of additional magnetic excitations in the magnetic long-range ordered state II. The silence of magnetic Raman scattering seems to be related to the incommensurate helimagnetic structure suggested in Ref. 11. In contrast to the 2M continuum from the Néel ordered state, the 2M continuum from singlet states shows no noticeable change in peak position as well as intensity as a function of temperature. This is due to the narrow bandwidth of triplet excitations compared to the magnitude of the spin gap. Moreover, two 2M continua are simply superposed to each other independently. This indicates that in phase II short-range singlet correlations and the helimagnetic ordered state coexist *coherently*. Furthermore, the simultaneous observation of magnetic excitations from Néel order and singlet correlations in phase I can be interpreted as the coherent coexistence of an antiferromagnetic long-range ordered and a dimerized state which are mutually exclusive. Note here that the dimerized state is robust in the course of the evolution of magnetic structures and their corresponding magnetic correlations. As mentioned above, such a coexistence has been reported in the impurity-doped spin-Peierls system  $\text{CuGeO}_3$  (Ref. 3) and the highly hole-doped quasi-1D cuprate  $\text{Sr}_{0.73}\text{CuO}_2$ .<sup>6</sup> The introduction of nonmagnetic impurities to dimerized states produces a local moment by breaking up dimers. With aid of higher-dimensional interactions long-range ordering occurs at low temperature.<sup>4</sup> This disorder-order transition scenario might be applicable to the studied system as the dimerized phase of  $\text{LiCu}_2\text{O}_2$  is intrinsically contaminated by a  $\text{LiCuO}$  impurity phase which has copper ions in a nonmagnetic  $\text{Cu}^+$  oxidation state. The  $\text{LiCuO}$  phase is estimated to be less than 10% of the total volume. It is arranged almost regularly in the form of platelets with the dimension of  $100 \times 7 \times 100 \text{ nm}^3$  (Ref. 10). It is

thus natural to expect that similar to a single-site dopant, such nanostructural nonmagnetic inclusions break  $\text{Cu}^{2+}$ - $\text{Cu}^{2+}$  bonding along the chains, enhance three-dimensional interactions, and eventually promote AFM long-range order at low temperatures.

However, within this mechanism it is difficult to capture the following features. First, the presence of a helimagnetic state is not explainable because for the introduction of dopants the interaction between local moments has an alternating sign. That is, its sign relies on whether the two local moments belong to the same or to opposite sublattices. As a result, frustrations are lifted and an AFM ordering is favored. Second, the transition of an incommensurate phase into the Néel ordered one at 9 K is driven by the presence of the magnetic  $\text{Li}_2\text{CuO}_2$  impurity.<sup>11</sup> Third, the 2M signal from a long-range ordered state is much stronger than that from a dimerized phase (see Fig. 2). All these observations indicate the predominance of a long-range ordering over a dimerization as well as the dependence of the magnetic structure on the kind of impurities, signaling the significant role of magnetic impurities. In the following we present a possible scenario.

Upon cooling dilute magnetic impurities which lie most probably between spin chains undergo long-range ordering via 3D interactions. Then, the long-range ordered impurities can be regarded as effective magnetic fields inducing long-range ordering in spin chains. The observed helimagnetic state is due to the compromise of AFM order with strong in-chain frustration. Furthermore, two successive transitions at 22.5 K and 24.2 K (Ref. 10) reflect an intriguing interplay of magnetic impurities between chains and nonmagnetic in-chain impurities on the background of the incommensurate spin structure. Upon further cooling, depending on the presence of the  $\text{Li}_2\text{CuO}_2$ -impurity, the Néel ordered phase will appear at about 9 K. This indicates that the collinear magnetic structure of the  $\text{Li}_2\text{CuO}_2$  impurity promotes the transition of the incommensurate phase to the commensurate one.

Finally, we will discuss the quasielastic Raman response observed above 10 K. Our experimental setup is carefully adjusted to suppress Rayleigh scattering. Therefore, the observed intensity is intrinsic and origins from fluctuations of the energy density of the system. Its presence is a remarkable feature of low-dimensional system with strong spin-phonon coupling.<sup>2</sup>

According to the theory of Reiter<sup>20</sup> and Halley,<sup>21</sup> the scattering intensity is given by the Fourier component of the correlation function of the magnetic energy density:  $I(\omega) \propto \int_{-\infty}^{\infty} dt e^{-i\omega t} \langle E(k,t) E^*(k,t) \rangle$ , where  $E(k,t)$  is the magnetic energy density. In a hydrodynamic assumption for the correlation function in the high temperature limit<sup>22</sup> the above equation is simplified to the Lorentzian profile  $I(\omega) \propto [C_m T^2 D_T k^2 / \omega^2 + (D_T k^2)^2]$ , where  $k$  is the scattering wave vector,  $D_T$  the thermal diffusion constant, and  $C_m$  the magnetic specific heat. In this case, magnetic specific heat is proportional to the integrated intensity divided by  $T^2$ . Using this relation one can map scattering intensity on thermodynamic quantities. Figure 4(a) displays integrated intensity of quasielastic scattering together with ESR intensity and static susceptibility as a function of temperature. There exists an

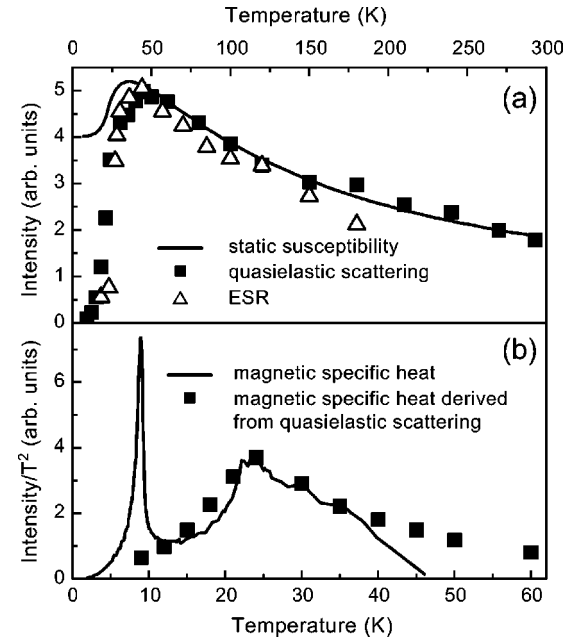


FIG. 4. (a) Comparison of the intensity of quasielastic scattering (full rectangle) and ESR (open triangle) to static susceptibility (solid line) taken from Ref. 10. (b) Mapping of the magnetic specific heat derived from quasielastic scattering (full rectangle) on the magnetic specific heat obtained by subtracting the phonon contribution (solid line).

overall good correspondence between integrated ESR and quasielastic intensity. However, they show a substantial deviation from the static susceptibility below 45 K. Here note that ESR probes excitations within excited states which originate from the low-dimensional character of interactions in  $\text{LiCu}_2\text{O}_2$  as the drastic drop of its intensity below 45 K shows. Thus, one can see that ESR and Raman spectroscopy are selectively sensitive to disordered short-range correlations. In contrast, the static susceptibility becomes dominated by 3D short-range-order antiferromagnetic correlations below 45 K. In Fig. 4(b) the magnetic specific heat derived from the quasielastic scattering is shown together with the magnetic part of specific heat obtained after subtracting a calculated phonon contribution from the measured specific heat. In the temperature interval  $12 \text{ K} < T < 40 \text{ K}$  there is a reasonable matching between them. The difference above 40 K can be attributed to an overestimation of the phonon contribution to the specific heat at high temperatures by choosing only one Debye function. The discrepancy below 12 K comes from the suppression of fluctuations of spin energy density in the Néel ordered phase.

A maximum of  $C_m$  can also provide an information on the exchange constant. In the case of 1D AF chain the magnetic specific heat has a broad maximum at  $k_B T \approx 0.481J$ . The frustration shifts the maximum of  $C_m$  to lower temperature,  $k_B T \sim 0.38J$ .<sup>23</sup> This results in  $J \sim 60 \text{ K}$  which is consistent with the value obtained from the peak position of the 2M scattering as well as from the static susceptibility.

In summary, a Raman scattering study of the frustrated spin chain compound  $\text{LiCu}_2\text{O}_2$  unveils a coexistence of

dimerized correlations and long-range order as a coherent superimposition of a dimerized state with a spin gap  $\Delta \sim 73$  K on a two-magnon continuum from a Néel ordered state shows. This is attributed to nanoscale sized magnetic/nonmagnetic defects. Moreover, the transition of a helimagnetic state into a Néel ordered one suggests a significant role of magnetic impurities in an incommensurate magnetic structure as a driving impetus to a commensurate structure. We

hope that our experimental observations will stimulate further theoretical investigations devoted to understanding magnetic properties of frustrated spin chain systems including magnetic/nonmagnetic defects.

The work was supported by Grants Nos. DFG/SPP 1073, INTAS 01-278, and NATO Collaborative Linkage Grant No. PST.CLG.977766.

- 
- <sup>1</sup>M. Hase *et al.*, Phys. Rev. Lett. **70**, 3651 (1993).  
<sup>2</sup>P. Lemmens *et al.*, Phys. Rep. **375**, 1 (2003).  
<sup>3</sup>L.P. Regnault *et al.*, Europhys. Lett. **32**, 579 (1995).  
<sup>4</sup>G.B. Martins *et al.*, Phys. Rev. Lett. **78**, 3563 (1997).  
<sup>5</sup>E.S. Sørensen *et al.*, Phys. Rev. B **58**, R14701 (1998).  
<sup>6</sup>G.I. Meijer *et al.*, Phys. Rev. B **60**, 9260 (1999).  
<sup>7</sup>R. Berger *et al.*, J. Alloys Compd. **184**, 315 (1992).  
<sup>8</sup>B. Roessli *et al.*, Physica B **296**, 306 (2001).  
<sup>9</sup>Vorotynov *et al.*, JETP **86**, 1020 (1998).  
<sup>10</sup>S. Zvyagin *et al.*, Phys. Rev. B **66**, 064424 (2002).  
<sup>11</sup>T. Masuda *et al.*, cond-mat/0310126 (unpublished); A.A. Gippius *et al.*, cond-mat/0312706 (unpublished).  
<sup>12</sup>M. Grove *et al.*, Phys. Rev. B **61**, 6126 (2000).  
<sup>13</sup>U. Kuhlmann *et al.*, Phys. Rev. B **66**, 064420 (2002).  
<sup>14</sup>Strictly speaking, the phase transition into a helimagnetic phase around 23 K consists of two successive transitions at 22.5 K and 24.2 K (Ref. 10). The possible origin will be discussed below.  
<sup>15</sup>P.A. Fleury *et al.*, Phys. Rev. **166**, 166 (1968).  
<sup>16</sup>M.G. Cottam and D.J. Lockwood, *Light Scattering in Magnetic Solids* (Wiley, New York, 1986).  
<sup>17</sup>P.A. Fleury *et al.*, Phys. Rev. Lett. **24**, 1346 (1970).  
<sup>18</sup>K.B. Lyons *et al.*, Phys. Rev. B **37**, 2353 (1988).  
<sup>19</sup>D.A. Tennant *et al.*, Phys. Rev. B **67**, 054414 (2003).  
<sup>20</sup>G.F. Reiter, Phys. Rev. B **13**, 169 (1976).  
<sup>21</sup>J.W. Halley, Phys. Rev. Lett. **41**, 1605 (1978).  
<sup>22</sup>B.I. Halperin *et al.*, Phys. Rev. **188**, 898 (1969).  
<sup>23</sup>H. Kuroe *et al.*, Phys. Rev. B **55**, 409 (1997).